



Coupled simulation of surface runoff and soil water flow using multi-objective parameter estimation

John Maximilian Köhne^{a,*}, Thomas Wöhling^{b,c}, Valérie Pot^d, Pierre Benoit^d, Sophie Leguédouis^{e,f}, Yves Le Bissonais^{e,g}, Jirka Šimůnek^h

^a Helmholtz Centre for Environmental Research – UFZ, Theodor-Lieser-Straße 4, D-06120 Halle (Saale), Germany

^b Lincoln Ventures Ltd., Lincoln Environmental Research Division, Private Bag 3062, Hamilton, New Zealand

^c Water and Earth Science Systems Research Centre, University of Tübingen, Institute for Geosciences, Sigwartstrasse 10, 72076 Tübingen, Germany

^d INRA, AgroParisTech, UMR 1091 EGC, F-78850 Thiverval-Grignon, France

^e INRA, UR0272, Unité de Science du Sol, Centre de Recherche Orléans, F-45075 Orléans Cedex 2, France

^f INRA, UMR Laboratoire Sols et Environnement, Nancy-Université, 2 Avenue de La Forêt de Haye, BP 172, 54505 Vandœuvre-lès-Nancy, France

^g INRA, UMR LISAH, 2 Place Pierre Viala, F-34060 Montpellier cedex 1, France

^h Department of Environmental Sciences, University of California Riverside, Riverside, CA, USA

ARTICLE INFO

Article history:

Received 28 September 2010

Received in revised form 7 March 2011

Accepted 1 April 2011

Available online 7 April 2011

This manuscript was handled by Dr. A. Bardossy, Editor-in-Chief, with the assistance of Vazken Andréassian, Associate Editor

Keywords:

Overland flow

Surface runoff

Multi-objective global parameter optimization

Mobile-immobile model

Simulation

Flow channel experiment

SUMMARY

A comprehensive description of water flow in environmental and agricultural systems requires an account of both surface and subsurface pathways. We present a new model which combines a 1D overland flow model and the 2D subsurface flow HYDRUS-2D model, and uses the multi-objective global search method AMALGAM for inverse parameter estimation. Furthermore, we present data from bench-scale flow experiments which were conducted with two 5-m long replicate soil channels. While rainfall was applied, surface runoff was recorded at the downstream end of the soil channel, subsurface drainage waters were sampled at three positions equally spaced along the channels, and pressure heads were recorded at five depths. The experimental observations were used to evaluate the performance of our modeling system. The complexity of the modeling approach was increased in three steps. First, only runoff and total drainage were simulated, then drainage flows from individual compartments were additionally evaluated, and finally a surface crust and immobile soil water were also considered. The results showed that a good match between measured and observed surface runoff and total drainage does not guarantee accurate representation of the flow process. An inspection of the Pareto results of different multiobjective calibration runs revealed a significant trade-off between individual objectives, showing that no single solution existed to match spatial variability in the flow. In spite of the observed crust formation, its consideration in the more complex model structure did not significantly improve the fit between the model and measurements. Accounting for immobile water regions only slightly improved the fit for one of the two replicate soil channels. Discrepancies between relatively complex model simulations and seemingly simple soil channel experiments suggest the presence of additional unknowns, such as heterogeneity of the soil hydraulic properties. Nevertheless, with its versatile subsurface options and powerful inverse method, the model system shows promise for studying hillslope flow problems involving both surface runoff and subsurface flow.

© 2011 Elsevier B.V. All rights reserved.

1. Introduction

Overland flow during storm events may affect the water and mass balance of environmental and agricultural systems. However, current vadose zone flow models include at most a simplified description of this process, such as instant removal of saturation/infiltration excess water as surface runoff (e.g., Ahuja et al.,

2000). As an alternative, combined models of overland and subsurface flow were developed.

The diffusion wave or kinematic wave approximations of the Saint-Venant equation are frequently used to describe overland flow, while the Green-Ampt or Richards equations are used to model infiltration or subsurface flow. Earlier approaches usually relied on analytical solutions, limiting their applications to relatively simple boundary conditions and homogeneous soil (Govindaraju et al., 1990; Wallach et al., 1997). Numerical solutions then allowed various generalizations, such as time-dependent boundary conditions (e.g., Govindaraju and Kavvas, 1991; Motha

* Corresponding author. Tel.: +49 345 5585 5406.

E-mail address: max.koehne@ufz.de (J.M. Köhne).

and Wigham, 1995; Woolhiser et al., 1990) or spatial variability of soil hydraulic properties (e.g., Corradini et al., 1998; Merz and Plate, 1997), and allowed consideration of runoff in addition to rainfall (e.g., Nahar et al., 2004). While many approaches relied on 1D overland flow and pseudo-2D (staggered independent 1D vertical columns) subsurface flow, extensions to two dimensions were also used for both overland flow (e.g., Gandolfi and Savi, 2000; Merz and Plate, 1997) and subsurface flow (e.g., Govindaraju and Kavvas, 1991; Singh and Bhallamudi, 1998). A 1D surface and quasi-3D subsurface (2D planes) model was introduced by Wöhling and Schmitz (2007) and successfully applied by Wöhling and Mailhol (2007). A comprehensive coupled 2D surface and 3D subsurface watershed model was introduced by Panday and Huyakorn (2004). A few models also considered the effect of infiltration and vertical gravity flow in macropores (e.g., Léonard et al., 2001; Merz and Plate, 1997), also in combination with heterogeneity in soil hydraulic properties (Herbst et al., 2006). A review of various surface–subsurface flow approaches has recently been presented by Furman (2008).

None of the above studies focused on inverse parameter identification, and most approaches do not even have a provision for inverse estimation. However, while prediction of vadose zone dynamics is already a challenge, adding surface flow to the model analysis further increases the complexity. The main problem is to characterize the spatial variability of soil hydraulic properties caused by variations in soil texture, structure, and layer interfaces (Kodesová et al., 2009; Kulli et al., 2003; Vogel et al., 2005), among other effects. The difficulty of independent model parameterization was the driving motivation behind exploring the benefit of using inverse parameter estimation in this study.

For parameter estimation of vadose zone models, local search methodologies are often employed that begin their iterative search from a single initial point in the parameter space. A prominent example is the nonlinear, gradient-based Levenberg–Marquardt search algorithm (Marquardt, 1963). However, such local derivative-based search methods often fail to evolve towards the global optimum in situations where the response surface exhibits multiple local optima in the parameter domain (e.g., Schwefel, 1993). In such cases, the final solution of the local search method is non-unique and essentially dependent on the starting point in the parameter space. While multi-start local search methods may help to overcome this problem under some circumstances, the convergence to the global solution cannot be guaranteed. As a response to this problem, global search algorithms were developed that use multiple concurrent searches from different starting points to efficiently reduce the chance of getting stuck in a single area of attraction (e.g., Deb et al., 2002; Madsen, 2003; Vrugt and Robinson, 2007).

Since any model is a simplification of reality and the underlying reality is never known exactly, model simulation results are inherently uncertain. One expression of this uncertainty is equifinality, characterized by multiple model structures and parameter sets yielding acceptable fits to observed data (Beven, 2006). To better understand the uncertainty and limitations of the model structure, the optimization problem can be formulated in a multi-objective context, where information contained in several data-sets is exploited simultaneously (Gupta et al., 1998; Vrugt et al., 2003; Wöhling and Vrugt, 2008). Among different multi-objective global parameter optimization procedures, A MultiAlgorithm Genetically Adaptive search Method (AMALGAM) developed by Vrugt and Robinson (2007) was found to be the most efficient algorithm for finding best attainable parameter sets with the least number of model evaluations (Wöhling et al., 2008).

The overall objective is to evaluate the usefulness of linking a surface flow model with a comprehensive vadose zone model (Simunek et al., 2003, 2008) and advanced multi-objective optimi-

zation techniques for studying the interacting flow–runoff behavior in a sloping soil. In this context, data from the controlled bench-scale flow experiment were utilized.

2. Material and methods

2.1. Overland flow model

The overland flow model is based on unpublished work by Šimůnek (2003). Hortonian overland flow is typically described using the kinematic wave equation, which is a simplification of the Saint-Venant equations and an excellent approximation of most overland flow conditions (Morris and Woolhiser, 1980; Singh et al., 2005; Woolhiser et al., 1990):

$$\frac{\partial h_o}{\partial t} + \frac{\partial Q_o}{\partial x} = R - I \quad (1)$$

where $h_o(x, t)$ is the unit storage of water (or mean depth for smooth surfaces) in the overland flow (L), $Q_o(x, t)$ is the overland discharge per unit width ($L^2 T^{-1}$), t is time (T), x is the distance coordinate over the soil surface (L), $R(x, t)$ is the local effective rainfall rate (rain minus evaporation) ($L T^{-1}$), and $I(x, t)$ is the local infiltration (or exfiltration) rate ($L T^{-1}$). The discharge Q_o per unit width can be calculated as follows:

$$Q_o = \alpha h_o^m \quad (2)$$

where $\alpha (L^{2-m} T^{-1})$ and $m (-)$ are parameters related to slope, surface roughness, and flow conditions (laminar or turbulent flow). Overland flow is often turbulent, with a large Reynolds number $Re = Q_o/\nu > 500$, where ν is the kinematic viscosity of water ($L^2 T^{-1}$). There is some evidence that turbulent flow conditions may prevail during rainfall even at lower Reynolds numbers (Deng et al., 2005). Flow for our experimental conditions was assumed to be turbulent and the coefficients in Eq. (2) were thus evaluated using the empirical Manning hydraulic resistance law and assuming $m = 5/3$ (Wallach et al., 2001):

$$\alpha = k \frac{S^{1/2}}{n_M} \quad (3)$$

where $S (-)$ is the slope, $n_M (-)$ is the Manning's roughness coefficient for overland flow, and k is a conversion constant which in SI units has the value of 1 and units of ($L^{1/3} T^{-1}$). From Eqs. (2) and (3) it can be seen that the n_M coefficient depends not only on surface roughness, but also on the slope and the overland discharge. For bare field soils, n_M typically ranges between 0.01 for a rather smooth surface (flat slope and slow overland discharge), and 0.2 for a rough soil surface (steeper slope and faster discharge) (Li and Zhang, 2001; Mohamoud, 1992; Sepaskhah and Bondar, 2002).

By substituting (2) into (1), and substituting $R - I$ by the net rate of local input, $q(x, t)$ ($L T^{-1}$), the following equivalent expressions describing overland flow are obtained:

$$\frac{\partial h_o}{\partial t} + \frac{\partial \alpha h_o^m}{\partial x} = q(x, t) \quad (4)$$

$$\frac{\partial h_o}{\partial t} + \alpha m h_o^{m-1} \frac{\partial h_o}{\partial x} = q(x, t) \quad (5)$$

A numerically stable, fully implicit four-point finite difference method, similar to the one used in the Kineros model (Woolhiser et al., 1990), was used to solve Eq. (1). The following discretization scheme was applied (subscript o is omitted for convenience).

$$\frac{1}{2} \left(\frac{h_i^{j+1} - h_i^j}{\Delta t} + \frac{h_{i+1}^{j+1} - h_{i+1}^j}{\Delta t} \right) + \varepsilon \frac{Q_{i+1}^{j+1} - Q_i^{j+1}}{\Delta x} + (1 - \varepsilon) \frac{Q_{i+1}^j - Q_i^j}{\Delta x} = \frac{1}{2} \varepsilon (q_i^{j+1} + q_{i+1}^{j+1}) + \frac{1}{2} (1 - \varepsilon) (q_i^j + q_{i+1}^j) \quad (6)$$

Subscripts *i* are nodal numbers, superscripts *j* and *j* + 1 represent previous and current times, Δ*t* and Δ*x* are temporal and spatial discretization steps, and ε is the temporal weighting coefficient; ε = 1 for the implicit scheme (the Crank–Nicholson scheme with ε = 0.5 gave similar results). The resulting nonlinear system of equations is solved using the Picard iterative approach, similar to the one used for the solution of the Richards equation in HYDRUS-2D (Šimůnek et al., 1999). The numerical model was validated by comparing its results with the corresponding analytical solution of Eqs. (4), (5) (Šimůnek, 2003).

The one-dimensional equation for overland water flow requires initial conditions, plus up to two boundary conditions; one for runoff (if any) at the upstream entrance and another for runoff at the downstream exit. The initial conditions for overland flow are represented by the initial ponding depths, *h*₀₀(*x*), assumed to be equal to the initial soil water pressure heads, *h*₀(*x*, *z*_{surf}), along the soil surface with the *z*-coordinate *z*_{surf}(*L*):

$$h_0(x, 0) = h_{00}(x) = h_0(x, z_{surf}) \quad \text{for } x, z_{surf} \in \Gamma_0 \quad (7)$$

when the pressure head is positive (the soil surface is ponded), or equal to zero when the pressure head is negative (the soil surface is unsaturated).

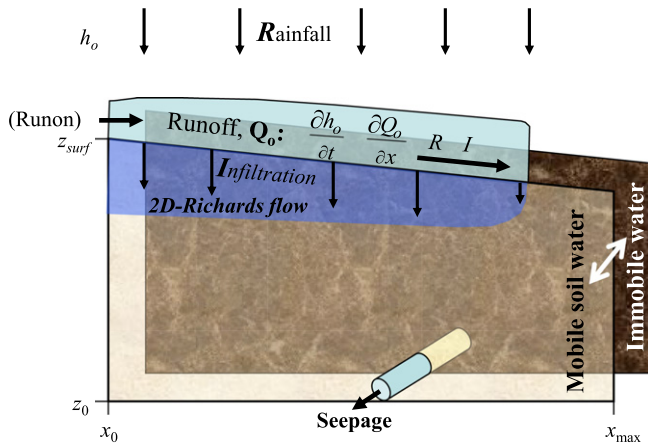


Fig. 1. Conceptual schematic of the coupled runoff-subsurface flow model based on HYDRUS-2D. An immobile region was assumed in the ‘MIM + Crust’ scenario, whereas in the remaining scenarios water in the entire soil domain was assumed to be mobile.

The boundary conditions for water flow represent water runoff at the entrance side (a Dirichlet boundary condition) with a prescribed ponding head, and a zero gradient for the ponding depth is assumed at the outlet side of the plot:

$$h_0(0, t) = h_{00} \quad \text{for } x = x_0, \quad t > 0 \quad (8)$$

$$\frac{\partial h_0(n, t)}{\partial x} = 0 \quad \text{for } x = x_n, \quad t > 0 \quad (9)$$

If there is no runoff, *h*₀₀(*t*) in (8) becomes zero. Since the lateral runoff discharge, *Q*_o, is calculated as a function of *h*₀ according to (2), the runoff is fully defined by Eq. (8), which is therefore equivalent with a flux-type (Neumann) condition.

The numerical solution of the overland flow equation was iteratively coupled with HYDRUS-2D (Šimůnek et al., 1999, 2008). Interactions with the HYDRUS-2D subsurface flow model are represented by the sink-source term *I* in Eq. (1). Coupling to overland flow is accomplished via dynamic atmospheric boundary conditions in the computation module of HYDRUS-2D as follows. During unsaturated conditions, there is no surface runoff and water infiltration is similar to the applied rainfall rate, which is described using a specified flux (Neumann) upper boundary condition. If the pressure at the surface exceeds zero, i.e. ponding occurs, then the upper boundary switches to a specified head (Dirichlet) condition (Šimůnek et al., 1999). Infiltration, *I*, is then calculated in the subsurface model using the Richards equation, where the pressure head in the subsurface domain at the upper boundary, *h*₀(*x*, *z*_{surf}), is assumed to be equal to the ponding water depth, *h*₀₀(*x*), which in turn is calculated as overland flow depth according to (1). The same Neumann–Dirichlet switch in boundary conditions was implemented for runoff at any location.

Finally, each drainage water outlet is represented by a single node at the bottom of the transport domain with a seepage face boundary condition. During each iteration, a saturated node of the potential seepage face is treated as a prescribed pressure head boundary with *h* = 0, while an unsaturated node is treated as a prescribed flux boundary with *Q* = 0. While in the former case the unknown boundary (drainage) flux *Q* is calculated, in the latter case the unknown pressure head is calculated.

The soil structure generally invokes zones of different water mobility in the soil. Often, preferential flow paths form highly mobile regions, contrasting with relatively immobile zones in the soil matrix. We coupled the model for overland flow with the dual-porosity mobile-immobile water model (assuming the saturation-based water transfer) in HYDRUS-2D. Then the pressure head in the mobile region at the surface is assumed to be equal to the ponding water depth, *h*₀₀(*x*). A schematic of the conceptual model is shown in Fig. 1. The model was set-up to represent the experimental system (Fig. 2).

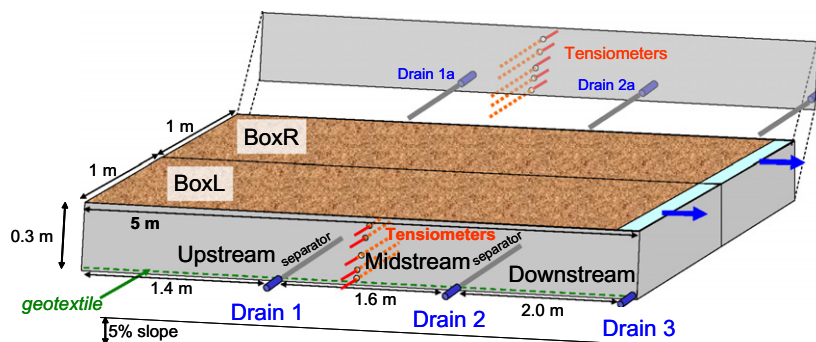


Fig. 2. Schematic overview of the soil channel. The grey lines denoted ‘separator’ represent metal sheets of a few cm height preventing lateral flow along the bottom between the up-, mid-, and down-stream segments.



Fig. 3. Photo of the soil flow channel at INRA Orléans.

2.2. Runoff experiment

2.2.1. Experimental set-up

A runoff experiment was conducted in the Soil Science Laboratory of the Institut National de la Recherche Agronomique (INRA) at Orléans (France). The experimental set-up was made of two replicate soil-filled boxes integrated in a channel of 5 m length, 2 m total width (1 m per replicate), and 0.3 m height, with a slope of 5% (Figs. 2 and 3). The left and right replicate boxes (Fig. 2) are subsequently referred to as BoxL and BoxR. They were filled with sieved soil obtained from a silt loam and silty clay loam, respectively. The experiment was designed to study the transport of pesticides with different sorbing properties as affected by interrill erosion (Leguédou et al., 2006; Leguédou and Bissonnais, 2004). In this study, however, we utilized only data from the silt loam soil, which carries the local designation 'Fontaine soil' and is found in the western part of the Paris Basin, Normandy (France). Fontaine soil has an aggregated structure, but aggregates are unstable and the soil is susceptible to erosion (Fig. 4) (Le Bissonnais et al., 1998; Leguédou and Bissonnais, 2004). The soil material was sampled from the Ap horizon of a plot on cultivated arable land near Fontaine (Bourville, Seine-Maritime), from a depth of 0–0.3 m.

Filling the soil boxes was accomplished in two steps, as follows. First, a 25-cm thick layer was built up by pouring dry-sieved (<5 cm aggregates) soil in 5-cm increments. Natural compaction of this 25-cm layer was realized by alternately applying about 10 recurring cycles of rainfall (until saturation) and drainage. Care was taken to avoid any ponding, erosion, or crust formation. When the soil stopped settling, the remaining 5 cm to the top were filled with sieved (<2 cm) soil in two 2.5-cm increments. This filling procedure invoked slight differences in the soil bulk density and water content with depth, as was measured on soil cores taken after the experiment (Table 1). The soil surface was reshaped into a furrow-

Table 1

Bulk densities of the Fontaine silt loam soil filled in the left (BoxL) and right (BoxR) channels.

BoxL			BoxR		
Depth (cm)	ρ_b (g/cm ³)	θ^a	Depth (cm)	ρ_b (g/cm ³)	θ^a
0–5	1.31	0.33	0–5	1.29	0.33
7.3–12.3	1.35	0.33	6.5–11.5	1.37	0.28
13.5–18.5	1.02	0.30	13–17	1.16	0.20
19.5–24.5	1.36	0.34	20–25	1.44	0.37
25–30	1.47	0.47	25–30	1.38	0.44

^a Water content measured a few hours after the end of the experiment.

ridge micro-topography (Leguédou and Bissonnais, 2004) parallel to the slope with a 2-cm height-amplitude and a 10-cm wavelength in a cross-section perpendicular to the slope (Fig. 4). The channel box was equipped with five tensiometers at five soil depths between 2 and 29 cm, centered at the mid position of $x = 2.5$ m.

The bottom of the box was covered with highly permeable geotextile. At upstream (1.4 m), midstream (3 m), and downstream (5 m) locations, metal sheets a few cm high at the bottom of the box impeded lateral flow along the bottom. They served as gutters channeling drainage water to the outlets (drains) representing different compartments, i.e., drain 1 – upstream (0–1.4 m), drain 2 – midstream (1.4–3 m), and drain 3 – downstream (3–5 m). Surface runoff was collected at the downstream end.

Soil hydraulic properties were independently measured in the lab on undisturbed field-sampled soil cores (1 dm³) using the Wind's (1966) method (Tamari et al., 1993). The Wind method yields uncertain results close to saturation, since the derived saturated hydraulic conductivity, K_s , is an extrapolated value. Additionally, K_s was measured using a permeameter method on samples of 1 dm³ in size (Table 2). The custom-made permeameter measured the saturated water flux for an imposed constant head as a function of time. The final steady-state flux was assumed to be equal to K_s .

Table 2

Soil hydraulic van Genuchten–Mualem parameters for measurements on the Fontaine silt loam soil (wind and permeameter measurements on undisturbed field samples; two replicates; permeameter measurements on box soil samples: mean \pm standard deviation for 10 measurements).

Wind's method (evaporation experiment)						Permeameter		
θ_r	θ_s	n	α	ρ_b	K_s	Field sample	Box sample	
			(1/cm)	(g/cm ³)	(cm/d)	(cm/d)	(cm/d)	
0.000	0.483	1.36	0.0112	1.37	12.2	16.3	146.0 \pm 43.6 ^a	
0.000	0.464	1.56	0.0105	1.34	12.8	16.3	9.1 \pm 5.5 ^b	

^a Soil samples below crust.

^b Soil with crust.



Fig. 4. The soil flow channel with aggregates and furrow-ridge surface micro-topography, prior to rainfall (left) and thereafter (mid). Detailed view of a cross-section through a rill revealing the surface crust (right).

Table 3

Mass balance information for the left (BoxL) and right (BoxR) soil boxes at the end of the first and second irrigation, respectively.

	Time (min)	Rain (l)	Runoff (l)	Drain 1 (l)	Drain 2 (l)	Drain 3 (l)	DrainΣ (l)	Storage (l)	DrainΣ (%)	Runoff (%)	Storage (%)
<i>First rain event</i>											
BoxL	32.5	79.9	9.1	0.0	0.0	0.0	0.0	70.8	0.0	11.4	88.6
BoxR	32.5	74.5	16.3	0.0	0.0	0.0	0.0	58.2	0.0	21.9	78.1
<i>Second rain event</i>											
BoxL	100	245.9	175.9	0.0	0.7	11.4	12.1	57.9	4.9	71.5	23.5
BoxR	100	229.2	197.9	3.2	14.2	16.4	33.9	-2.5	14.8	86.3	-1.1

However, since hydraulic properties measured for undisturbed soil may not represent the sieved soil material used for filling the soil box, additional permeameter measurements were also conducted on soil samples (5 cm height and diam.) collected from the box after the experiments. Samples were taken from mini-furrows with surface crust (11 measurements) and from small ridges (10 measurements) (Table 2). Samples taken from ridges had an order-of-magnitude higher K_s than samples taken from furrows. The surface crust thus strongly reduced K_s . However, K_s of samples from ridges were also much larger than K_s measured on field samples. A possible explanation is that the filling procedure may have caused development of inter-aggregate regions that had increased K_s . Moreover, a relatively small sample size may have caused an overestimation of mean K_s and its variability (Mallants et al., 1997).

2.2.2. Experiment

Two rainfall events were applied to each of the replicate soil boxes. The rainfall simulator was designed to simulate rain events of spatially uniform intensity. It was made of five oscillating nozzles at 1.1 m horizontal spacing and was placed at 6.4 m above the soil surface. The device produced raindrops with 1.3 mm median diameter and a kinetic energy of $16 \text{ J mm}^{-1} \text{ m}^{-2}$. The rainfall intensity received by the box was verified by placing a plastic sheet on the soil surface and measuring the runoff. The spatial variability of the rain intensity was measured within the experimental area using rainfall gauges; the coefficient of variation was 15%. The mass balance for both rainfall events and the two soil boxes is given in Table 3. The rainfall rate differed slightly between 29 mm/h (147.6 l/h) for BoxL (the total surface area of 5.09 m^2), and 28.4 mm/h (137.5 l/h) for BoxR (the total surface area of 4.84 m^2). The difference between left and right surface areas is due to an imprecision when dividing the box into two parts by placing a metal sheet of 5 m length in the middle. The width of BoxL is 1.02 m (upstream) and 1.015 m (downstream), while for BoxR it is 0.97 m (upstream) and 0.975 m (downstream), respectively.

The first rainfall was applied to pre-wet the soil and did not produce any drainage. Runoff started after 20 min and 21 min for the left and right boxes, respectively. Rainfall was stopped after 32.5 min when the surface runoff rate reached 10% of the applied rainfall rate. Rapid formation of a seal crust in the mini-furrows was visually observed within 10 min of the first simulated rainfall. In the crust, boundaries between aggregates disappeared and the surface appeared smoother and of lighter color (Fig. 4). After a 24-h interruption, the second rainfall of 100 min was applied, using the same rate as for the first event.

2.3. Multi-objective optimization

2.3.1. Theory

The aim of the inverse modeling procedure is to find values of model parameters that provide the best attainable fit between model simulation and corresponding observations. The multi-

objective framework used herein comprised three different criteria:

$$\min F(\mathbf{u}) = \begin{bmatrix} F_1(\mathbf{u}) \\ F_2(\mathbf{u}) \\ F_3(\mathbf{u}) \end{bmatrix} \quad (10)$$

where F_1 to F_3 are defined as the normalized Root Mean Square Error (nRMSE) objective functions of the differences between observed and simulated drainage fluxes at the midstream (F_1) and lower (F_2) drains, and the surface runoff (F_3) collected at the lower end of the sand box, and \mathbf{u} is the vector of model parameters to be estimated. Here, \mathbf{u} includes both the soil hydraulic van Genuchten–Mualem (VGM) parameters (van Genuchten, 1980) and the Manning's roughness coefficient, n_M , usually a not well-known overland flow parameter.

A normalization is required to compensate for differences in magnitude and variability of the objective functions, i.e., to balance their weights in the global search. The objective function values are transformed so that the minima of the objectives in the initial sample of parameter sets exhibit a similar distance to the origin (Madsen, 2000; Mertens et al., 2004; Wöhling and Vrugt, in press):

$$F_i = \frac{f_i}{\sigma_i} + \phi_i \quad i = 1, 2, 3 \quad (11)$$

where f_j is the non-transformed (RMSE) objective function, σ_j is the standard deviation associated with f_j of the initial sample, and ϕ_j is a transformation constant given by

$$\phi_i = \max \left[\min \left(\frac{f_j}{\sigma_j} \right), j = 1, 2, 3 \right] - \min \left(\frac{f_i}{\sigma_i} \right) \quad i = 1, 2, 3 \quad (12)$$

The AMALGAM method (A MultiAlgorithm Genetically Adaptive search Method), recently developed by Vrugt and Robinson (2007), was used for parameter estimation of the coupled surface–subsurface model. AMALGAM is a population-based global search algorithm that combines two concepts of a simultaneous multi-algorithm search method with genetically adaptive offspring creation for estimating the Pareto set of solutions of a given multi-objective inverse problem. The Pareto optimal or Pareto efficient solutions represent trade-offs among different objectives, having the property of moving from one solution to another results in the improvement of one objective while causing deterioration in one or more of the others (Gupta et al., 1998; Vrugt et al., 2003). An illustrative summary of the basic features of AMALGAM appears

Table 4

Optimization scenarios. MIM – mobile and immobile regions. The + sign indicates an objective.

Scenario	Uniform-2	Uniform-3	MIM + Crust
Objectives	2	3	3
Runoff	+	+	+
Total drainage	+	–	–
Midstream drainage	–	+	+
Downstream drainage	–	+	+

in Wöhling et al. (2008), while a more detailed description can be found in Vrugt and Robinson (2007), and is therefore not repeated here.

2.3.2. Optimization procedure and scenarios

A reliable model simulation requires the realistic definition of initial and boundary conditions. Boundary conditions were set equal to the applied rainfall rate. Initial conditions were defined

in terms of an equilibrium pressure profile, which was estimated by interpolating measured tensiometer values.

Scenarios with different complexities should reveal the effects of data available for model optimization, and of particular soil properties. Among the six scenarios originally studied, three distinct scenarios were selected for this paper (Table 4). The 'Uniform' scenarios were built upon the assumption of homogeneous soil hydraulic properties in the entire domain, represented by a single set of VGM parameters. The 'Uniform-2' scenario includes two

Table 5
Range of the optimized parameters.

Parameters	θ_s	n	α (1/cm)	K_s (cm/d)	τ^b	n_M	$\theta_{s,m}^a$	$\theta_{s,m}^a$	ω^a (1/d)
Min	0.15	1.001	0.001	0.000144	-3	0.0001	0.05	0.05	0
Max	0.70	9 (4 ^a)	2 (1 ^a)	14,400	3	0.5	0.5	0.5	1

^a Only in the MIM + Crust scenario.

^b Exponent in the van Genuchten Mualem model.

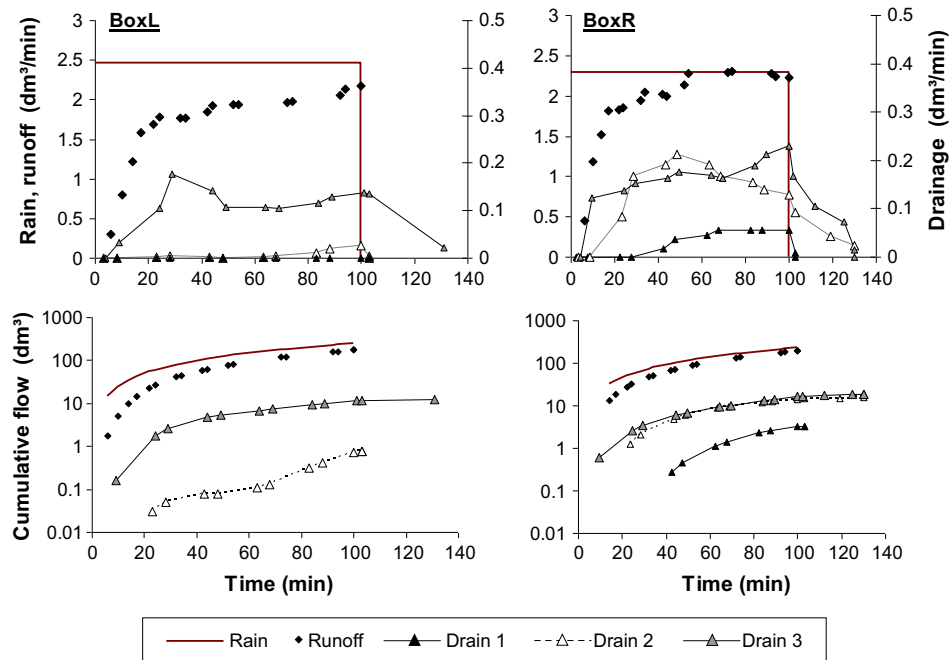


Fig. 5. Experimental data for the BoxL (left) and BoxR (right) replicates as measured during the second rainfall event. Applied rainfall, surface runoff, and drainage at three drains are given in terms of rates (top) and cumulative flows (bottom), respectively.

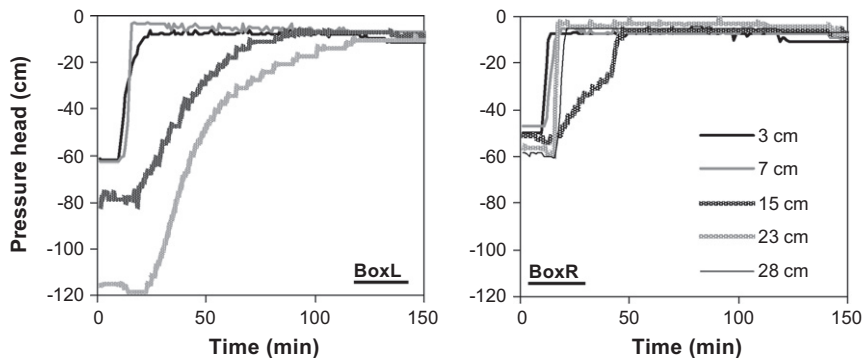


Fig. 6. Pressure head response to rainfall as observed at different depths using tensiometers installed in the middle of the replicates BoxL and BoxR.

objective functions for runoff and total drainage, i.e., the sum of the three individual drainage flows. This reduces Eq. (10) to two components, i.e., F_1 for drainage and F_2 for runoff. The ‘Uniform-3’ scenario includes three objective functions as defined in Eq. (10). Both scenarios were compared to assess the potential importance of using spatially resolved subsurface flow information.

The ‘MIM + Crust’ scenario considers mobile and immobile regions in a soil with a thin crust layer placed on top of the soil. Crust formation was observed during the experiment. The presence of mobile and immobile regions was assumed to be an effective way of accounting for any type of flow heterogeneity, such as fingering flow in the layered soil system, inhomogeneous infiltration due to the micro-funneled surface, or inter-aggregate percolation through the aggregated soil. Furthermore, the ‘MIM + Crust’ optimization includes 3 objective functions. Additionally, a ‘Crust’ (without MIM) scenario was simulated, but since its results did not yield much additional information, we did not report them.

From the resulting Pareto surface, we selected four Pareto points. The first three Pareto points were the best individual solu-

tions with respect to the individual objectives, which are henceforth denoted as Pareto extremes, \hat{F}_i . There is one Pareto extreme for midstream drainage (\hat{F}_1), one for downstream drainage (\hat{F}_2), and one for runoff (\hat{F}_3). The extremes are a subset of the Pareto optimal or efficient solutions defined above. The fourth Pareto point is subsequently referred to as the compromise solution, where the sum of all three normalized root mean square error objectives, F_i , is at its minimum (\hat{F}_0):

$$\hat{F}_0 = \min \sum_{i=1}^3 F_i(\mathbf{u}) \quad (13)$$

Only data for the second rain event for both BoxL and BoxR were used, since the first rain event produced only little runoff and drainage. For the same reason, drainage (drain 1) at the upstream position was not considered. Flux data for the recession phase and tensiometer recordings were not included in the parameter estimation, but were utilized for independent model performance evaluation.

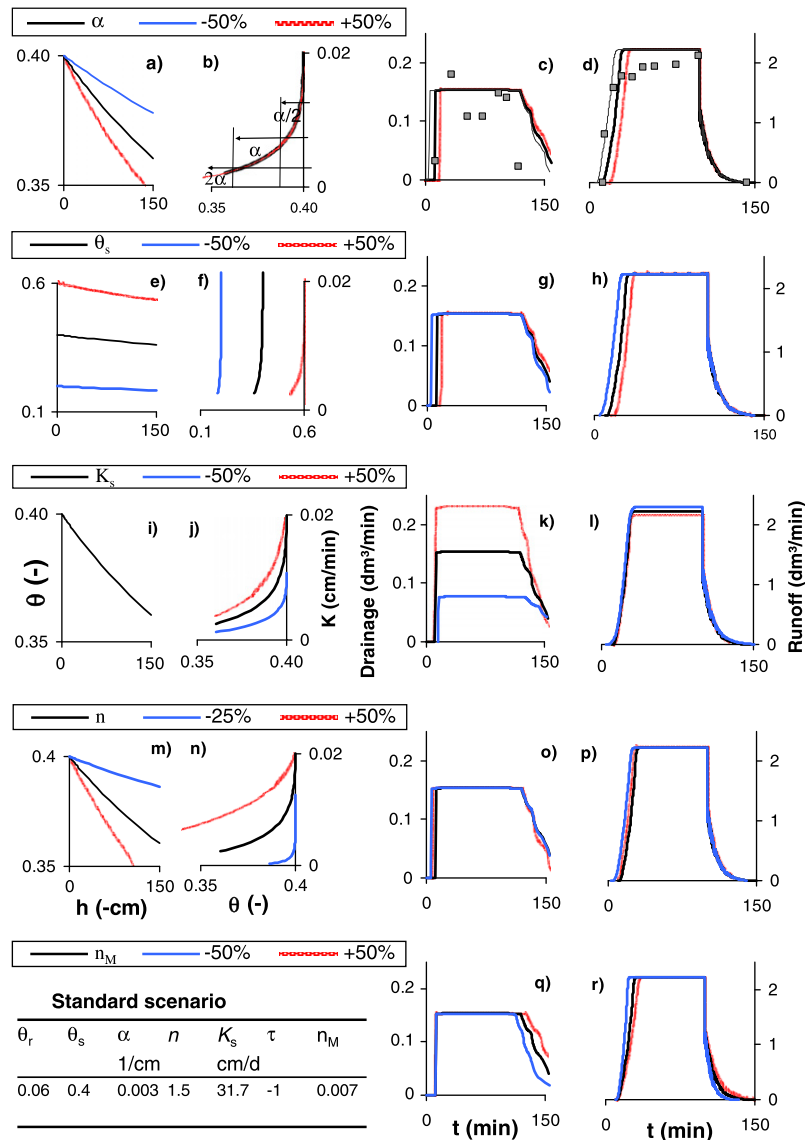


Fig. 7. Hydraulic functions (left) and corresponding model simulation results for surface runoff and subsurface drainage (right) based on different parameters α (a–d), θ_s (e–h), K_s (i–l), n (m–p), and Manning’s n_M (q and r).

The different AMALGAM scenarios described herein were terminated after the algorithm converged on a stable Pareto surface, which occurred within 20,000–50,000 model evaluations, depending on the number of converging runs. Each scenario required 1–2 weeks of run time in sequential mode using the Matlab R2008a

(64 bit) Microsoft Windows™ XP Professional (64 bit) modeling environment on a Dell™ Precision 390 workstation with a Quad-Core Intel® Core™2 Extreme processor QX6700 (2.67 GHz) and 4 GB of RAM. The run time could be reduced by at least a factor of three by running AMALGAM in parallel mode on all four cores of the workstation. The goodness-of-fit was evaluated by comparing (i) simulated and observed runoff and drainage, and (ii) \hat{F}_i values of Pareto extreme and compromise solutions in the objective function space as visualized in Pareto plots.

The total number of optimized parameters depended on the scenario (Table 5). In the VGM model, the relation $m = 1 - 1/n$ was assumed, along with an air entry value of -2 cm (Ippisch et al., 2006). The residual water content was set to zero, $\theta_r = 0$. With these assumptions, six parameters remained to be optimized in the uniform scenario. These include Manning's roughness coefficient, n_M , and five VGM parameters: the saturated water content, θ_s (-), the curve shape parameters n (-) and α (L^{-1}), the saturated hydraulic conductivity, K_s ($L T^{-1}$), and the exponent in the hydraulic conductivity mode, τ (-). The 'MIM + Crust' scenario considers mobile and immobile soil water regions. Here, a version of the MIM model was chosen in which the mass transfer between domains is based on differences in saturation instead of pressure head (Köhne et al., 2004; Simunek et al., 2003). With the residual water content assumed as zero, the only additional parameters are the mobile and immobile saturated water contents, $\theta_{s,m}$ and $\theta_{s,im}$, and the transfer coefficient, ω . Thus, the 'MIM + Crust' scenario required 14 parameters, i.e., n_M and ω plus the set of six parameters ($\theta_{s,m}$, $\theta_{s,im}$, n , α , K_s , τ) for both the soil and crust. A large range was assigned to each parameter to permit AMALGAM to search the entire possible space (Table 5).

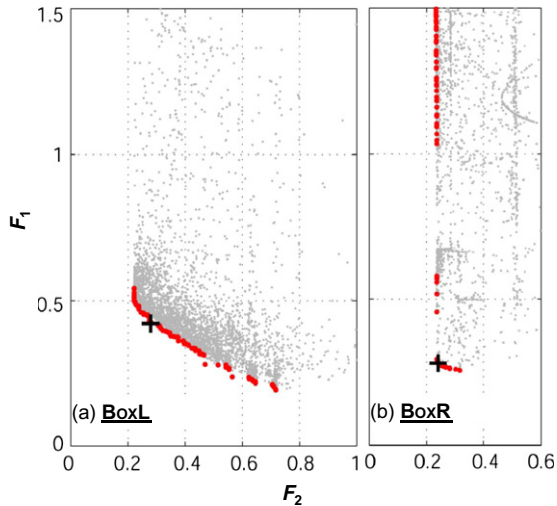


Fig. 8. Uniform-2 scenario (two objective functions): Pareto trade-off planes between objective functions F_1 (runoff) and F_2 (total drainage rate) for (a) BoxL and (b) BoxR. Small grey dots – Pareto solutions, Big (red) dots – Pareto optimal solutions, a cross – compromise solution. (For interpretation of the references to colour in this figure legend, the reader is referred to the web version of this article.)

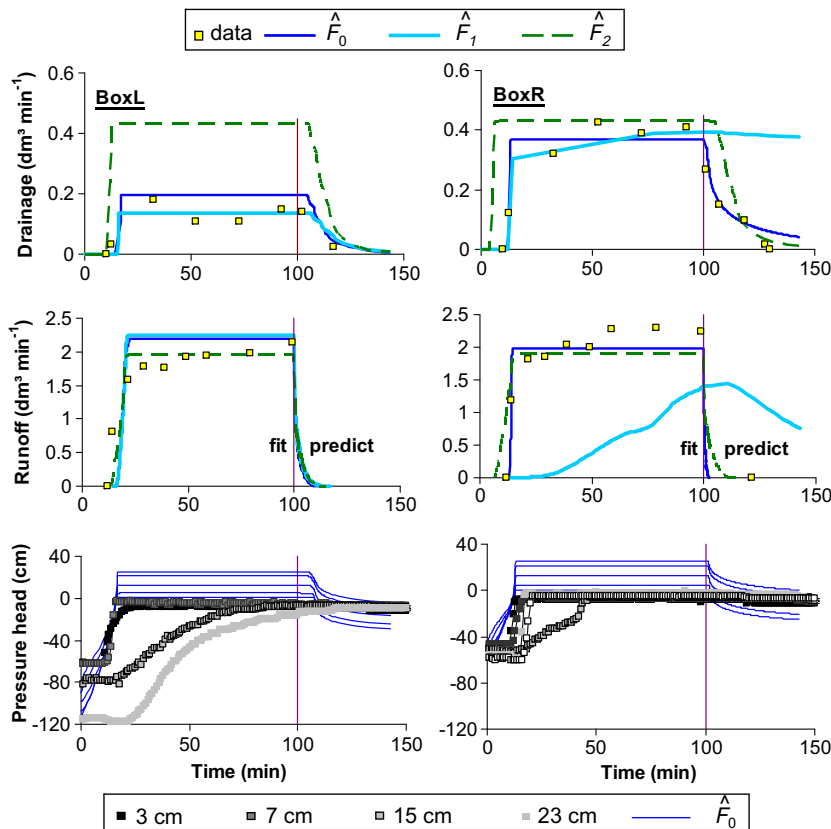


Fig. 9. Uniform-2 scenario (two objective functions): observations and simulations based on parameters at the Pareto extreme solutions for drainage (\hat{F}_1) and surface runoff (\hat{F}_2), and the compromise solution (\hat{F}_0). The objective function comprised only runoff and drainage until 100 min. Later observations and pressure heads are predictions. The pressure head prediction is shown based on the compromise solution.

3. Results

3.1. Experimental results

Only the second rainfall event was studied, since the first event did not produce any drainage and pressure head values indicated very inhomogeneous moisture distribution prior to the first event. Fig. 5 shows the experimental data for the second rainfall event, including runoff and drainage responses in both replicates. Surface runoff and drainage began approximately 5 min after the start of rainfall. Final steady flow rates of about 2 dm³/min were 10 times larger for surface runoff than for the largest drainage rates, which were observed at the downstream drains (Fig. 5). The sum of cumulative drainage and runoff from BoxR was approximately equal to the rainfall amount of the second experiment after 100 min. For BoxL, a gap of 57 dm³ (23%) in the water balance suggests a water content increase of 0.038. This hypothesis was qualitatively confirmed by the increase of pressure heads during a rainfall event (Fig. 6). For BoxL, initial pressure heads ranged between –60 cm and –120 cm (Fig. 6a), suggesting more unsaturated moisture conditions than in BoxR, where values of –50 to –60 cm were measured (Fig. 6b). Moreover, in BoxL, the initial response times for the pressure heads increased with soil depth and showed a slow increase at depths below 7 cm. By contrast, the tensiometers in BoxR showed a rapid succession of their initial response, and the increase at the 23- and 28-cm depths was faster than at the 15-cm depth (Fig. 6b), suggesting preferential flow in more permeable soil regions embedded in less permeable ('immobile') regions. The 15-cm depth was characterized by a low bulk density and relatively dry moisture content recorded a few hours after the experiment (Table 1). Apart from preferential flow caused by surface topography or layer interfaces, filling the box with sieved (<5 cm) soil aggregates might have created inter-aggregate flow paths. Pressure heads could then show more rapid or slower response, depending on whether the tensiometer is located in or between soil clods. Such immobile soil regions could also explain the incongruity between the apparently closed water balance for BoxR and the observed increase in pressure heads suggesting an increase in water storage. Since immobile regions saturate and drain more slowly than the remaining soil, they may not have reached equilibrium during the experiment.

After an initial fast increase, the surface runoff rate slowly continued to increase. This gradual increase in the runoff rate implies a related decrease in the infiltration rate, which in turn suggests a

corresponding decrease of surface hydraulic conductivity over time. Indeed, the erosion of soil particles and the formation of a crust on the soil surface were observed during the first rainfall event, particularly for BoxL. During the experiment this crust may have further settled and compacted, with a concurrent decrease in the soil surface hydraulic conductivity. For BoxR, a noticeable increase of the runoff rate at approximately 50 min coincides with the lowest pressure head measurement (at a 15-cm depth) reaching saturation. While replicate experiments will never show identical results, the differences between the hydraulic responses of the two boxes appear to be larger than would be expected from a random variation. Both received identical pre-treatment with 10 rainfall events. So what is the explanation that the two boxes do not show more similar results? The differences in bulk densities (Table 1) suggest either some spatial variability in the soil reconstruction or some heterogeneity in the soil material.

Limited data were also collected to characterize the recessing limb of the drainage and runoff hydrographs after the end of rainfall at 100 min (Fig. 5). For BoxR, drainage ceased within 2, 20, and 30 min, at drains 1–3, respectively (Fig. 5c), which is the opposite sequence of the onset of drainage at the beginning (Fig. 5d). For BoxL, drainage was essentially zero for drain 1, ceased within 2 min for drain 2, and lingered for 30 min for drain 3.

3.2. Model sensitivity

A qualitative sensitivity study was conducted in order to assess the effect of changing parameter values on the simulation results for runoff and drainage fluxes. The VGM parameters α , θ_s , K_s , n , τ , and Manning's n_M of the base case scenario were obtained by manually calibrating the model to observations from BoxL (Fig. 7). The calibrated parameters are mostly within the range of experimental values (Table 2). For sensitivity analysis, all parameters were varied by +/-50%. As an exception, the lower threshold for n was set to -25%, since n has to be larger than unity. Using the same relative variations for all parameters has the advantage of giving a quick first impression of the sensitivity. However, the results need to be seen in the light of differing range of parameter values for describing different soils. This range is often smallest for θ_s , larger for n , α , τ , n_M , and largest for K_s . Fig. 7 shows the changes in the soil hydraulic functions and model responses to a change in the input parameter values. Hydraulic functions are plotted in terms of $\theta(h)$ and $K(\theta)$, since $\theta(h) - K(h)$ and $S_e(h) - K(S_e)$ do not respond to a variation of some of the parameters.

Table 6

Optimized parameters for the uniform scenario with two objectives optimization. RMSE – normalized root mean square error, F_0 – compromise solution, F_r – Pareto extreme for simulated runoff, F_d – Pareto extreme solution for the simulation of total drainage.

Pareto results	θ_s	n	α (1/cm)	K_s (cm/d)	τ	n_M	F_1	F_2	F_Σ
<i>BoxL</i>									
F_d	0.451	1.80	0.00324	28.2	-2.99	0.0011	0.222	0.542	0.764
F_r	0.405	1.51	0.00285	90.6	-1.34	0.0019	0.717	0.194	0.911
F_0	0.467	1.83	0.00322	41.3	1.74	0.0008	0.281	0.421	0.702
<i>BoxR</i>									
F_d	0.467	1.66	0.00506	76.5	-0.41	0.114	0.226	2.462	2.688
F_r	0.499	1.37	0.00489	63.5	0.88	0.0001	0.316	0.256	0.574
F_0	0.500	1.37	0.00489	77.6	0.91	0.0001	0.240	0.281	0.521
<i>BoxL – manual calibration (Fig. 7)</i>									
	0.4	1.5	0.003	31.7	-1	0.007			
<i>Measured</i>									
	θ_s	n	α	K_s					
				Wind		Permeameter (field)		Permeameter (lab)	
	0.483	1.36	0.0112	12.2		16.3		146.0 ± 43.6 ^a	
	0.464	1.56	0.0105	12.8		16.3		9.1 ± 5.5 ^b	

^a Soil samples with crust.

^b Soil below crust.

Decreasing α shifts the point of the steepest slope of $\theta(h)$ towards more negative (larger absolute) values of h (van Genuchten, 1980). Hence, within the pressure head range of the experiment, decreasing α increases $\theta(h)$. While changing α does not affect the shape of the $K(\theta)$ curve, decreasing α indirectly increases $K(\theta)$ by limiting it to a more saturated range (Fig. 7a and b). Accordingly, the soil saturates faster, leading to an earlier start of drainage (Fig. 7c) and runoff (Fig. 7d).

A variation of θ_s by $\pm 50\%$ results in seemingly very different hydraulic functions (Fig. 7e and f), which invoke almost the same flow responses as corresponding changes of α (Fig. 7g and h). The explanation is that when α or θ_s are reduced, the slope of $\theta(h)$ is less steep in both cases, so that $K(\theta)$ stays closer to its saturated endpoint, K_s .

Doubling or bisecting the value of K_s itself (Fig. 7i and j) does not affect the onset and cessation of flows more than α or θ_s . However, K_s is the single parameter that controls the partitioning between runoff and drainage at saturated steady-state conditions (Fig. 7k and i). When additionally considering its potentially largest range of variation, K_s emerged as the most sensitive parameter.

The variation of n shows relatively complex results. As opposed to α or θ_s , a decrease in n increases $\theta(h)$ and decreases $K(\theta)$. The net effect on flows is not unidirectional; both a decrease by 25% or an increase by 50% lead to an earlier onset of runoff and drainage. An increase of n by 25% (not shown) would show a very similar onset of runoff and drainage as the standard scenario.

When Manning's roughness parameter, n_M , is decreased so as to represent a smoother surface, this leaves drainage onset unaffected (Fig. 7q), but causes a more rapid rise of runoff to its maximum value (Fig. 7r). The recessions in both runoff and drainage are accelerated by a decrease in n_M (Fig. 7r and q).

Finally, in this particular scenario, the tortuosity parameter, τ , had practically no effect on both $K(\theta)$ and simulated flows. Nevertheless, τ was included in the global optimization, since it cannot be asserted that τ will not show significant effects when the values of the other VGM parameters differ. In the inverse analysis, a wide range was chosen for all parameters in order to sample all possible values. For τ this range was set from -3 to $+3$.

3.2.1. Uniform-2 scenario

The Uniform-2 scenario considers a homogeneous soil and two objective functions, i.e., F_1 (F_2) based on the normalized RMSE between simulated and observed total drain flow (runoff). First, inverse model results are studied in terms of the F_1 – F_2 Pareto plane (Fig. 8). Among all F_1 – F_2 pairs (grey dots), the Pareto efficient parameter solutions (red solid circles) form Pareto fronts, which look different for the two replicates. For BoxL (left panel of Fig. 8), the front is diagonal. For BoxR, the Pareto front shows a distinct corner located at $F_1 = 0.24$ and $F_2 = 0.27$, representing the compromise solution, \hat{F}_0 . These comparable values for F_1 and F_2 suggest a successful normalization. For BoxR, a parameter set can be identified that fits both normalized objective functions equally well. This is not the case for BoxL, where the Pareto front exhibits a more distinguished trade-off between F_1 and F_2 .

Observations and the corresponding model simulations are compared in Fig. 9. The trade-off between Pareto extreme solutions for BoxL is clearly illustrated (Fig. 9, left panel): a reduction in drainage goes along with an increase in surface runoff, and vice versa. For both Pareto extremes, the respective complementary fluxes were overestimated. Accordingly, the compromise solution, \hat{F}_0 , slightly overestimates both drainage and surface runoff by some 5%. This reveals that for scenario 1 and BoxL, no parameter set exists for which the flow model will accurately represent the experiment. Simulation results could be improved if experimental data were not considered as error-free, but to some extent uncertain. For example, if a 5% lower effective rainfall rate was assumed

in the model input, to account for lateral spray losses as suggested by the slight gap in the water balance, model optimization would certainly better match runoff and drain flow observations for BoxL.

For BoxR (Fig. 9, right panel), the Pareto extremes invoked very different flow simulations. The model with parameters at Pareto extreme \hat{F}_1 incorrectly predicted prolonged drainage after the end of rainfall (where data were not included in the optimization), along with an entirely wrong runoff pattern. The \hat{F}_0 compromise solution fitted both runoff and drainage well, and also predicted drainage recession.

The prediction of pressure heads, which were not included in the model calibration, is shown in Fig. 9 (bottom panels). The simulations match the initial tensiometer response quite well. However, some observed pressure heads lag considerably behind others. As discussed previously, some soil regions appear to be less accessible to infiltrating water, which cannot be represented in the model that assumes uniform homogeneous conditions. Moreover,

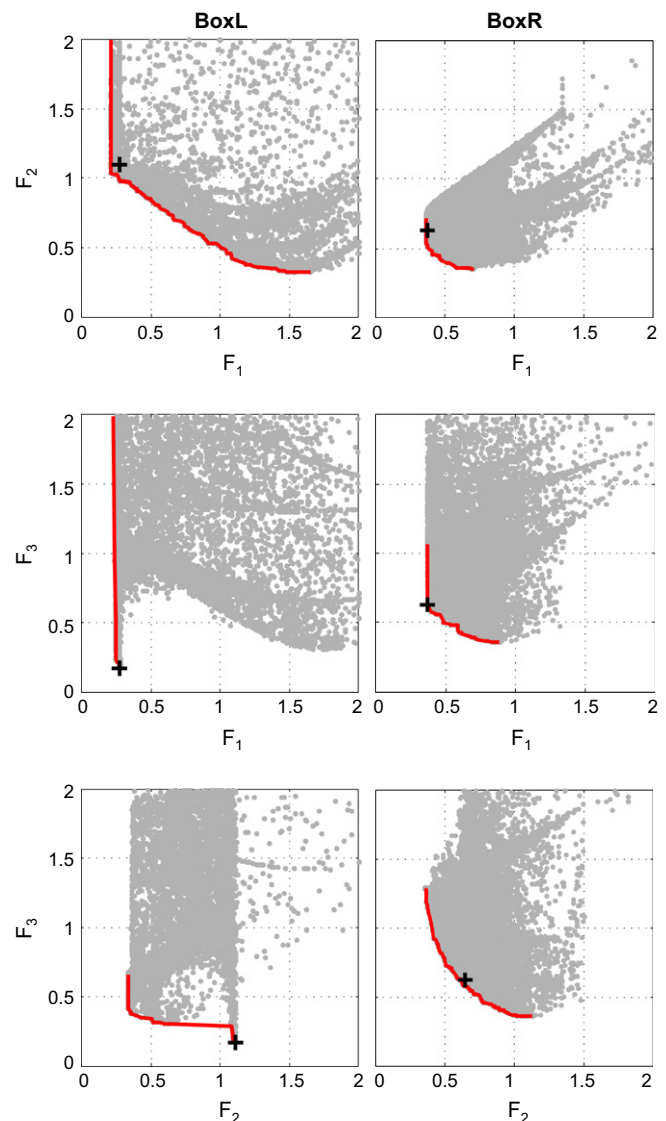


Fig. 10. Uniform-3 scenario (three objective functions): Pareto trade-off planes between three combinations of objectives for BoxL (36,000 evaluations) and BoxR (50,000). Pareto optimal solutions – red line of narrowly spaced dots; a cross – compromise solution. Objectives F_1 and F_2 refer to cumulative drainage at the mid- and down-stream drain, respectively; F_3 refers to surface runoff. (For interpretation of the references to colour in this figure legend, the reader is referred to the web version of this article.)

observed maximum values for pressure heads below zero reveal that there was no buildup of water pressure with depth during conditions of ponding. By contrast, the simulation shows positive pressures during ponding. Inserting a thin, highly conductive drainage layer to mimic the geotextile below the soil would remove positive pressures from the simulation (not shown).

Optimized parameter values are shown in Table 6. For comparison, the manually calibrated values (BoxL) and those obtained in the experimental measurements are displayed also in Table 6. Most VGM parameters do not deviate much between the F_0 compromise solutions and independent measurements. The optimized K_s values ranged between those measured on furrow and ridge samples (Table 6). The Manning’s roughness parameter was very small, $n_M < 0.001$, suggesting an even surface. The surface of this artificially prepared soil was indeed smooth compared to arable soils in their natural settings. However, the effects of funneled runoff pattern due to the interrill micro-topography may have been lumped into the Manning’s n_M parameter. In the experiment, surface runoff was somewhat accelerated by being confined to slope-parallel mini-furrows, whereas the model assumed sheet flow covering the entire soil surface. The confinement of surface flow to a smaller fraction of the soil surface may lead to a smaller effective value of the Manning’s n_M parameter. We tried to mimic

this effect by assuming only half the width of the box. The optimization then produced a n_M value increased by some 10%, while θ_s doubled, and other VGM parameters changed considerably (not further shown).

3.2.2. Uniform-3 scenario

The Uniform-3 scenario was defined by a search of three Pareto extremes (see Eq. (10)). The bi-criterion F_1-F_2 , F_1-F_3 , and F_2-F_3 surfaces of the three-dimensional Pareto trade-off space (objective space) are shown in Fig. 10 for BoxL and BoxR, respectively. There is no common minimum for all three objectives for both replicates. For BoxR, the bi-criterion fronts exhibit a curved shape, with the compromise solution getting equal shares of normalized RMSE from all objective functions (Fig. 10).

The observed and simulated cumulative runoff and drainage at three drains are compared in Fig. 11. Cumulative data were used in the optimization in an attempt to force it to match the mass balance of the observed volumetric flows. The compromise solution \hat{F}_0 for BoxL (Fig. 11, left) fails to match midstream drainage, but fits downstream drainage and surface runoff. The \hat{F}_1 Pareto extreme matched only up- and midstream drainage well. The results demonstrate that for this model scenario there is no \hat{F}_0 for BoxL that fits all three objectives simultaneously.

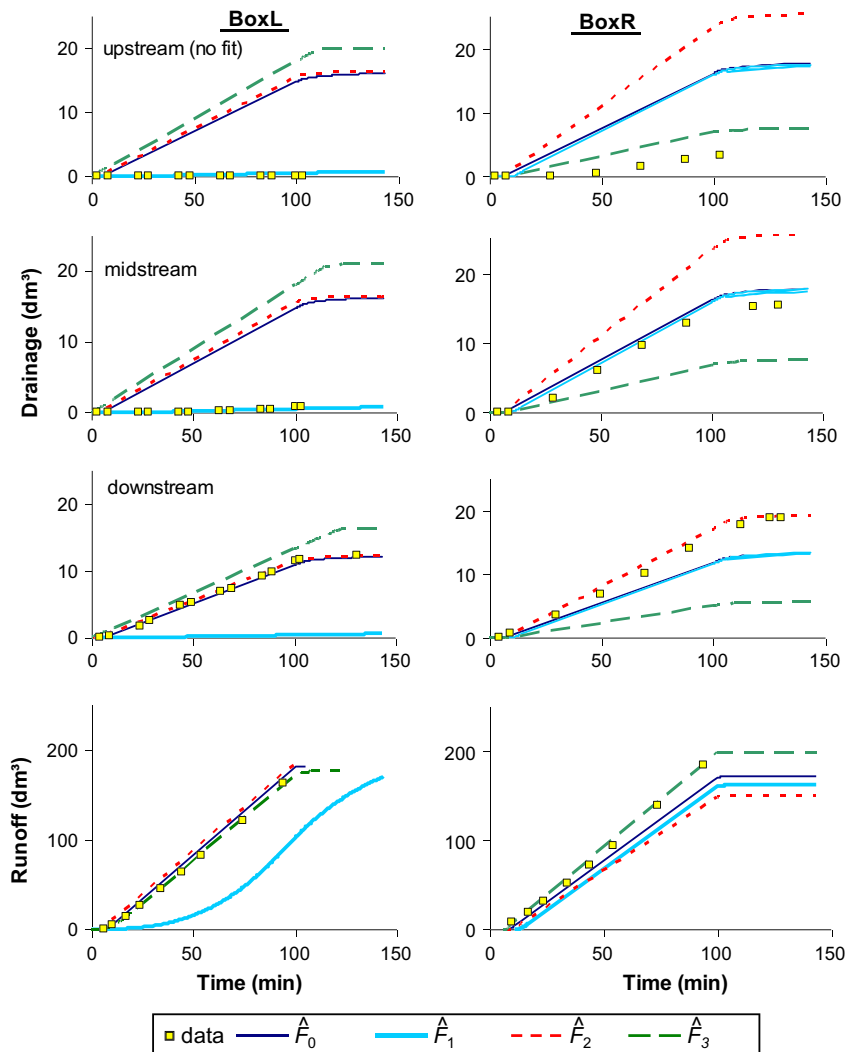


Fig. 11. Uniform-3 scenario (three objective functions): observed cumulative surface runoff and drainage at up-, mid-, and down-stream drains, and model simulation results for different Pareto extreme solutions for drainage at midstream (F_1) and downstream (F_2) drains, surface runoff (F_3), and the compromise solution (F_0), for BoxL (left) and BoxR (right).

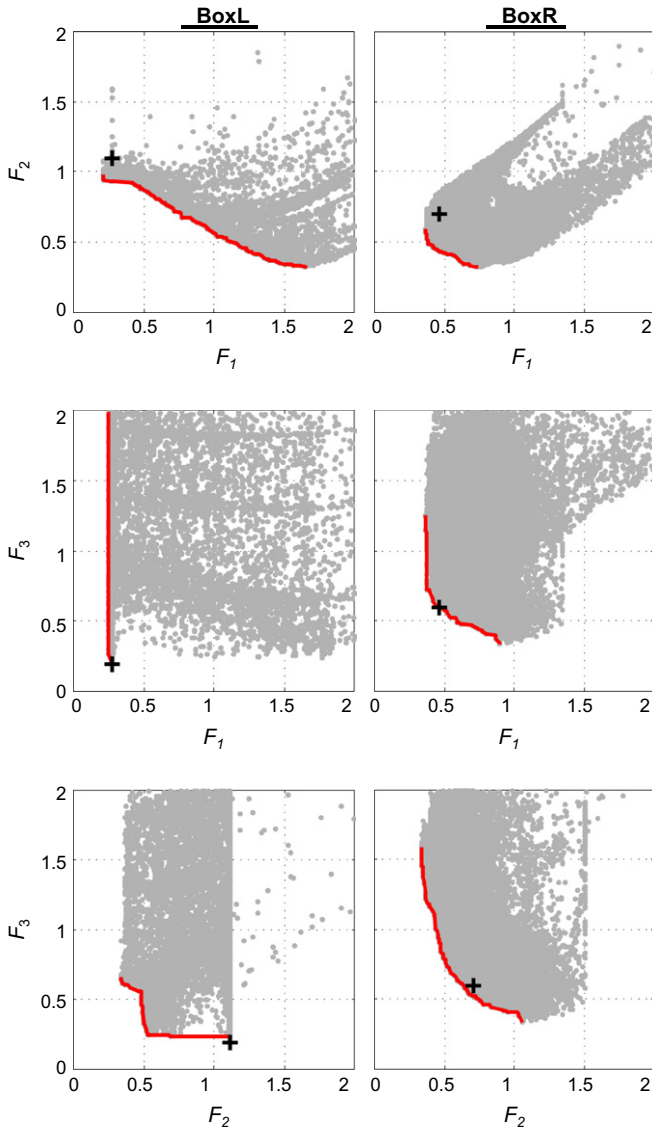


Fig. 12. MIM + Crust Scenario: Pareto trade-off planes between three combinations of objectives for BoxL (21,200 evaluations) and BoxR (50,040). Front of red dots – Pareto optimal solutions; a cross – compromise solutions with the constraint $K_s(\text{crust}) < K_s(\text{soil})$. Objectives F_1 and F_2 refer to cumulative drainage at the mid- and downstream drains; F_3 refers to surface runoff.

Table 7

Optimized parameters for the Uniform-3 and MIM + Crust Scenarios with three objectives optimization. F_m , F_1 , F_r – Pareto extreme solutions for the simulation of drainage from the midstream and downstream drains, and for runoff, respectively.

Pareto result	Uniform-3 (BoxL)				Uniform-3 (BoxR)			
	F_1	F_2	F_3	F_Σ	F_1	F_2	F_3	F_Σ
F_m	0.21	2.71	3.65	6.57	0.36	0.73	1.07	2.16
F_1	1.65	0.33	0.66	2.64	0.70	0.35	1.29	2.34
F_r	0.27	1.10	0.18	1.55	0.88	1.12	0.36	2.36
F_0	0.27	1.10	0.18	1.55	0.37	0.64	0.63	1.63
	MIM + Crust (BoxL) ^a				MIM + Crust (BoxR) ^a			
F_m	0.27	0.99	3.65	4.90	0.37	0.65	1.01	2.02
F_1	2.01	0.46	1.31	3.78	0.76	0.35	1.52	2.62
F_r	1.84	0.66	0.37	2.87	0.90	1.07	0.39	2.36
F_0	0.77	0.72	0.90	2.40	0.46	0.71	0.59	1.76

^a With constraint $K_s(\text{crust}) < K_s(\text{soil})$.

In contrast, \hat{F}_0 better represents the different BoxR data (Fig. 11, right). This is because the increase of drainage towards the downstream end is not as extreme as in the BoxL replicate. The Pareto extreme for midstream drainage, \hat{F}_1 , agrees with the observations nearly as well. The minimal upstream drainage is difficult to explain and points to heterogeneity in the material properties at the surface or subsurface. Upstream drainage was not included in the fitting procedure, but is shown for completeness.

The inverse simulation reveals that even a relatively good match of surface runoff and lumped drainage (Uniform-2 scenario) does not guarantee a correct model description of the spatial pattern of subsurface flow.

3.2.3. MIM + Crust scenario

The ‘MIM + Crust’ scenario considers mobile and immobile regions in a soil with a surface crust. This scenario, motivated by the aggregated structure of the soil and observed crust formation, again includes the three objectives for overland flow and mid- and downstream drainage. The bi-criterion fronts of the 3D Pareto trade-off space (Fig. 12) look very similar to those obtained for the Uniform-3 scenario (Fig. 11). We note that a constraint was imposed to keep the saturated hydraulic conductivity of the crust below that of the soil ($K_s(\text{crust}) < K_s(\text{soil})$), which was obtained for only 1053 runs out of 20,000 for BoxL and 14,030 runs out of 50,040 for BoxR. This constraint filtered out some slightly lower Pareto extremes for the MIM model, effectively without the surfaced crust. Overall, the Pareto extremes and the compromise solution did not improve the results compared to the Uniform-3

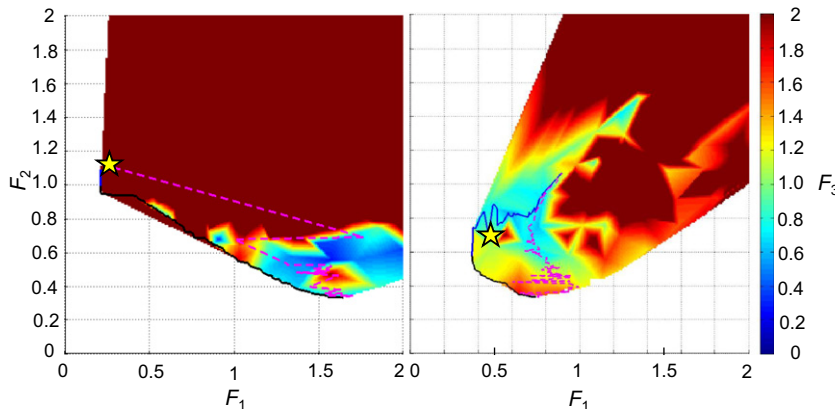


Fig. 13. MIM + Crust scenario: the objective function (F_1 – F_3) space; the color code indicates F_3 . Left: BoxL, Right: BoxR. The black solid line shows the F_1 – F_2 front of the Pareto optimal solutions, the dark solid line depicts the F_1 – F_3 Pareto front, the hatched purple line indicates the F_2 – F_3 Pareto front, and the stars represent the Pareto compromise solution, \hat{F}_0 .

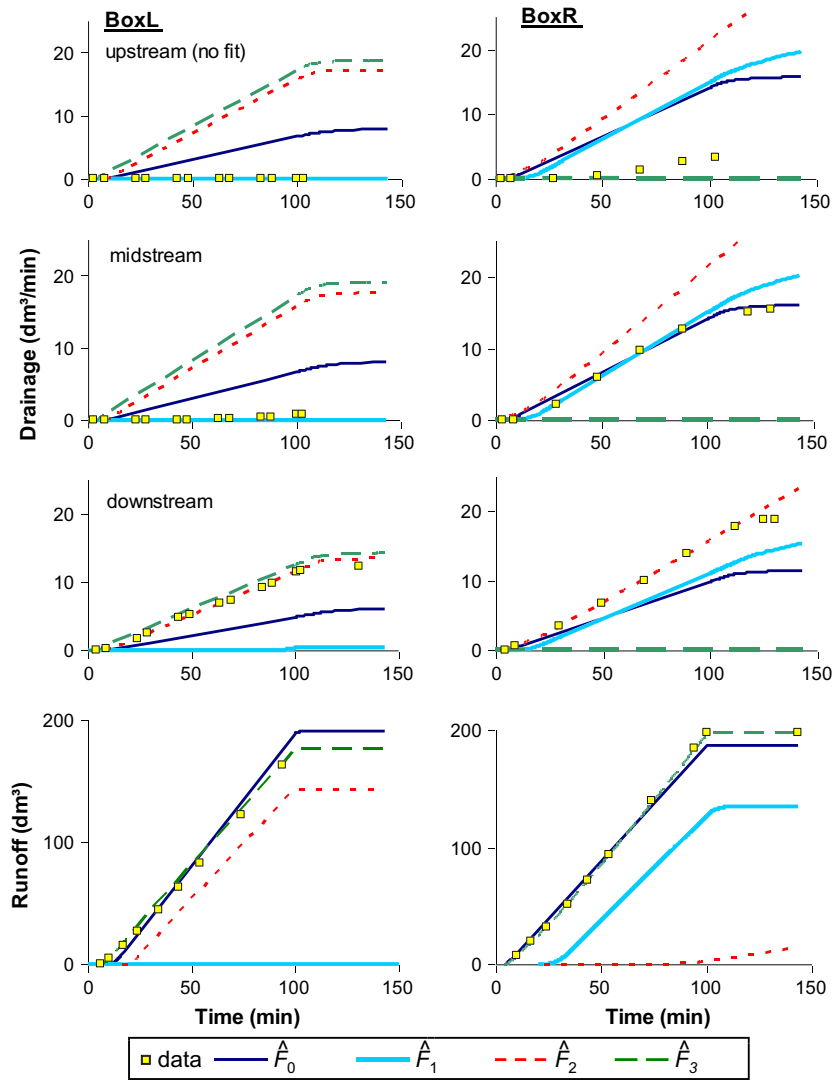


Fig. 14. MIM + Crust scenario (three objective functions): observed cumulative surface runoff and drainage at up-, mid-, and down-stream drains, and model simulation results for different Pareto extremes for drainage at midstream (\hat{F}_1) and downstream drain (\hat{F}_2), surface runoff (\hat{F}_3), and the compromise solution (\hat{F}_0), for BoxL (left) and BoxR (right).

example (Table 7). A more compact visualization of the objective space is shown in Fig. 13 for the F_1 – F_2 Pareto trade-off plane with the color coded objective F_3 . Visually, cumulative midstream drainage and runoff were fitted slightly better for BoxR (Fig. 14) than in the Uniform-3 scenario (Fig. 12), but the differences were rather small.

Since no compromise solution could be found that would match all data equally well, the optimized model parameters may not be meaningful, and were thus omitted. Hence, the added model complexity did not result in an improved match. If a local optimization approach had been chosen, such as Levenberg Marquardt, it would not have been possible to rule out a failure in the inverse procedure behind this lack of agreement. Using multi-objective optimization proved that there was a discrepancy between model structure and experimental data.

Fig. 15 compares simulated surface runoff depths, h_o , for the different scenarios at nine observation points along the surface. Maximum values for h_o are less than 2.5 mm. For a given overland discharge rate, Q_o , the depth h_o increases with n_M (Eqs. (2) and (3)). Hence, the differences between simulated h_o originate mostly from differences in the fitted n_M values, since the optimized values for Q_o did not differ that much. For each scenario, h_o increases

downhill. The onset of runoff, in response to rainfall, occurs almost simultaneously at different positions along the slope. Some scenarios differ with regard to the recessing limbs after the stop of rainfall. Only those scenarios with relatively high h_o show faster dissipation in the upslope part.

4. Discussion

In our case study, the task was to match drainage flows at mid- and downstream hillslope positions and runoff. A ‘validation’ test was added to predict (without fitting) the pressure heads, the recession part of drainage flows, and the drainage hydrographs at the upstream position. However, an increase in drainage in the downslope direction could not be reproduced by any of the considered model scenarios. This could have been caused by soil layers with different soil bulk densities that may have generated saturated lateral flow on layer interfaces. Such a situation, which could be captured by explicit consideration of layers in the model, was not simulated because of the considerable increase in the number of calibration parameters.

The use of a global optimization technique rules out the fitting procedure itself as a possible pitfall. Since model assumptions were

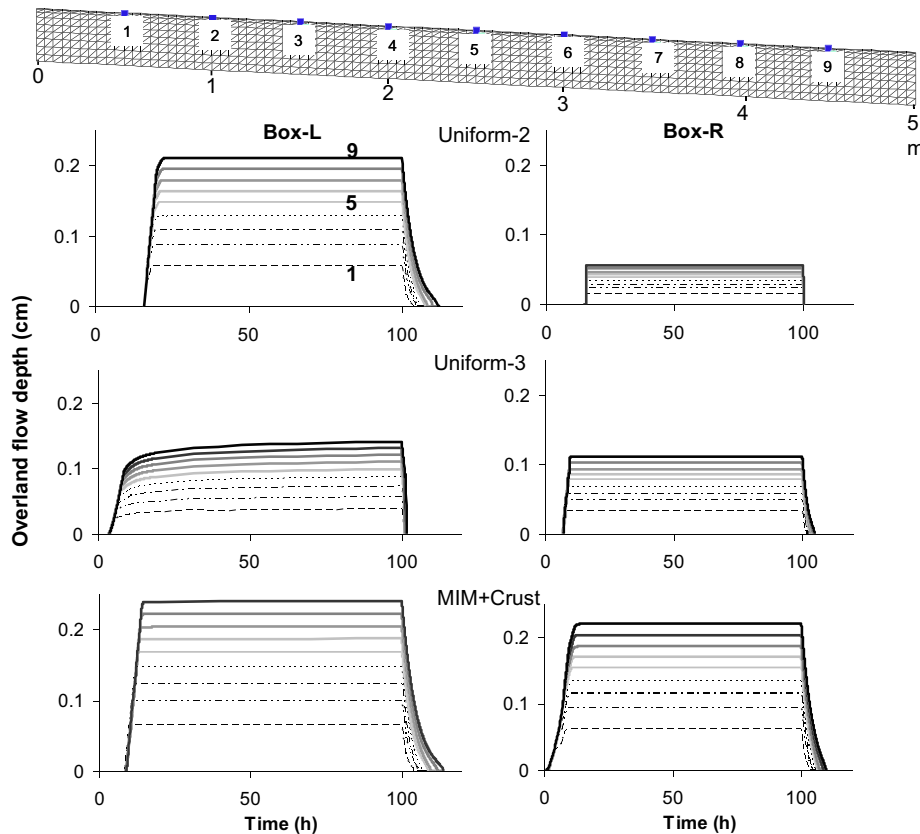


Fig. 15. Overland flow depths simulated at different observation nodes (numbers in the top figure) along the upper boundary of HYDRUS-2D for different compromise scenarios for BoxL (left) and BoxR (right).

explicitly known, the difficulty of simultaneously matching all different data suggested the presence of some sort of heterogeneity of soil hydraulic or surface properties that developed despite of the highly controlled environment. The aggregated and layered soil showed erosion and crust formation at the surface. The consideration of a crust, although observed, was not highly relevant in the flow simulation. Had the development of the crust been more pronounced upstream than downstream, this could have explained the increase in drainage flux towards the lower half of the box. The spatial and temporal development of a surface crust and its effect on infiltration was indeed measured and simulated recently (Augeard et al., 2007), although on a much smaller soil system. This kind of analysis was beyond the scope of this study. However, if available, such information could be fed into the model.

The AMALGAM multi-objective global search method was useful for proving that there was no common optimal parameter set that described all observations at different spatial locations equally well. The shape of the Pareto trade-off space illustrates clearly the incommensurateness of the objective functions. The analysis thus revealed the divergence between model structure or hypothesis, and the experimental observations. In our case, the assumption of having uniform and isotropic soil, or aggregated soil with crust, does not accurately represent the spatial nature of the flow process. Further information with regard to parameter uncertainty could be gained by studying the parameter ranges for Pareto solutions (e.g., Wöhling et al., 2008).

In vadose zone modeling, there is a large body of literature on including different types of observations into the model calibration and its effects on parameter identification (e.g., Friedel, 2005; Vrugt et al., 2008; Wöhling and Vrugt, in press; Zhang et al., 2003). However, to the best of our knowledge, similar studies involving coupled surface–subsurface flow are so far missing.

Similar results, which we obtained for different scenarios and parameter sets (Uniform-3 and MIM + Crust), point to the well-known equifinality problem, where several underlying model structures may yield similar simulation results (Beven, 2006). Reasons are, among others, the incomplete knowledge of the natural system and its inaccurate representation in the model. To account for this type of uncertainty, (Klaus and Zehe, 2010) suggested to include multiple structural set-ups of a physically based model, e.g., by employing the Generalized Likelihood Uncertainty Estimation method (Klaus and Zehe, 2010).

5. Conclusions

A coupled surface–subsurface flow model based on HYDRUS-2D (Šimůnek et al., 1999) was presented and linked to the multi-objective parameter search method AMALGAM (Vrugt and Robinson, 2007). Further, results from a highly controlled bench-scale experiment of surface and drainage flows in response to rainfall was presented. The data were used to evaluate the model performance and to test various hypotheses regarding different flow processes. Multi-objective parameter estimation with different normalized RMSE objective functions, Pareto trade-off space analysis, and visual comparison between model results and experimental observations were jointly used in this procedure.

The following conclusions can be drawn. Coupled surface–subsurface flow is a complex problem which requires model calibration to match several types of observations related to runoff and soil water dynamics. While there is a large body of literature related to inverse estimation for vadose zone models, more research seems necessary to extend these techniques also to coupled models. To this end, the AMALGAM technique, along with Pareto plot

analysis, was a useful tool for global optimization and for studying trade-off patterns between multiple objectives. In our case study, it showed that a common optimal parameter set to describe all types of observations equally well did not exist.

The result could be used to rethink the design of experimental set-ups and model structures. Moreover, the analysis revealed that a good match between simulated and observed surface runoff and total drainage does not guarantee an accurate representation of the flow process.

Overall, the suggested model appears useful for studying the hydraulics of overland flow and subsurface flow in sloping soils, potentially up to a hillslope scale. The multi-objective model calibration adds a powerful method for understanding the role of different hydraulic processes in such systems.

Acknowledgements

The helpful comments and suggestions of two anonymous reviewers are highly appreciated. Funding of this work was provided by the German Research Foundation (DFG) under contract DFG KO2899-1. The authors wish to thank the technical assistance of B. Renaud and L. Prud'homme for rainfall simulations. They also thank F. Darboux and C. Legout for their scientific help in the rainfall experiments.

References

- Ahuja, L.R., Rojas, K.W., Hanson, J.D., Shaffer, M.J., Ma, L., 2000. Root Zone Water Quality Model – Modeling Management Effects on Water Quality and Crop Production. Water Resources Publications, LLC, Highlands Ranch, CO, p. 372.
- Augeard, B., Assouline, S., Fonty, A., Kao, C., Vauclin, M., 2007. Estimating hydraulic properties of rainfall-induced soil surface seals from infiltration experiments and X-ray bulk density measurements. *J. Hydrol.* 341 (1–2), 12–26.
- Beven, K., 2006. A manifesto for the equifinality thesis. *J. Hydrol.* 320 (1–2), 18–36.
- Corradini, C., Morbidelli, R., Melone, F., 1998. On the interaction between infiltration and Hortonian runoff. *J. Hydrol.* 204 (1–4), 52–67.
- Deb, K., Pratap, A., Agarwal, S., Meyarivan, T., 2002. A fast and elitist multiobjective genetic algorithm: NSGA-II. *Trans. Evol. Comput.* 6, 182–197.
- Deng, Z.-Q., de Lima, J.L.M.P., Singh, V.P., 2005. Transport rate-based model for overland flow and solute transport: parameter estimation and process simulation. *J. Hydrol.* 315 (1–4), 220–235.
- Friedel, M.J., 2005. Coupled inverse modeling of vadose zone water, heat, and solute transport: calibration constraints, parameter nonuniqueness, and predictive uncertainty. *J. Hydrol.* 312 (1–4), 148–175.
- Furman, A., 2008. Modeling coupled surface–subsurface flow processes: a review. *Vadose Zone Journal* 7 (2), 741–756.
- Gandolfi, C., Savi, F., 2000. A mathematical model for the coupled simulation of surface runoff and infiltration. *J. Agric. Eng. Res.* 75 (1), 49–55.
- Govindaraju, R.S., Kavvas, M.L., 1991. Dynamics of moving boundary overland flows over infiltrating surfaces at hillslopes. *Water Resour. Res.* 27 (8), 1885–1898.
- Govindaraju, R.S., Kavvas, M.L., Jones, S.E., 1990. Approximate analytical solutions for overland flows. *Water Resour. Res.* 26 (12), 2903–2912.
- Gupta, H.V., Sorooshian, S., Yapo, P.O., 1998. Toward improved calibration of hydrologic models: Multiple and noncommensurable measures of information. *Water Resour. Res.* 34 (4), 751–763.
- Herbst, M., Diekkrüger, B., Vanderborght, J., 2006. Numerical experiments on the sensitivity of runoff generation to the spatial variation of soil hydraulic properties. *J. Hydrol.* 326 (1–4), 43–58.
- Ippisch, O., Vogel, H.J., Bastian, P., 2006. Validity limits for the van Genuchten–Mualem model and implications for parameter estimation and numerical simulation. *Adv. Water Resour.* 29 (12), 1780–1789.
- Klaus, J., Zehe, E., 2010. Modelling rapid flow response of a tile-drained field site using a 2D physically based model: assessment of 'equifinal' model setups. *Hydrol. Process.* 24 (12), 1595–1609.
- Kodesová, R., Vignozzi, N., Rohosková, M., Hájková, T., Kocárek, M., Pagliai, M., Kozák, J., Šimunek, J., 2009. Impact of varying soil structure on transport processes in different diagnostic horizons of three soil types. *J. Contam. Hydrol.* 104 (1–4), 107–125. doi:10.1016/j.jconhyd.2008.10.008 (Special Issue "Flow Domains").
- Köhne, J.M., Köhne, S., Mohanty, B.P., Šimunek, J., 2004. Inverse mobile–immobile modeling of transport during transient flow. *Vadose Zone J.* 3 (4), 1309–1321.
- Kullli, B., Stamm, C., Papritz, A., Fluhler, H., 2003. Discrimination of flow regions on the basis of stained infiltration patterns in soil profiles. *Vadose Zone J.* 2 (3), 338–348.
- Le Bissonnais, Y., Benkhadra, H., Chaplot, V., Fox, D., King, D., Daroussin, J., 1998. Crusting, runoff and sheet erosion on silty loamy soils at various scales and upscaling from m² to small catchments. *Soil Tillage Res.* 46 (1–2), 69–80.
- Leguédou, S., Bissonnais, Y.L., 2004. Size fractions resulting from an aggregate stability test, interrill detachment and transport. *Earth Surf. Proc. Land.* 29 (9), 1117–1129.
- Leguédou, S., Benoit, P., Pot, V., Le Bissonnais, Y., 2006. A 10-m² Laboratory Lysimeter to Assess Lateral and Vertical Pesticide Transfers in a Plowed Horizon. *Geophysical Research Abstracts*. European Geosciences Union, Vienna, p. 1.
- Léonard, J., Perrier, E., de Marsily, G., 2001. A model for simulating the influence of a spatial distribution of large circular macropores on surface runoff. *Water Resour. Res.* 37 (12), 3217–3225.
- Li, Z., Zhang, J., 2001. Calculation of field manning's roughness coefficient. *Agric. Water Manage.* 49 (2), 153–161.
- Madsen, H., 2000. Automatic calibration of a conceptual rainfall-runoff model using multiple objectives. *J. Hydrol.* 235 (3–4), 276–288.
- Madsen, H., 2003. Parameter estimation in distributed hydrological catchment modelling using automatic calibration with multiple objectives. *Adv. Water Resour.* 26 (2), 205–216.
- Mallants, D., Mohanty, B.P., Vervoort, A., Feyen, J., 1997. Spatial analysis of saturated hydraulic conductivity in a soil with macropores. *Soil Technol.* 10 (2), 115–131.
- Marquardt, D.W., 1963. An algorithm for least-squares estimation of nonlinear parameters. *J. Soc. Ind. Appl. Math.* 11 (2), 431–441.
- Mertens, J., Madsen, H., Feyen, L., Jacques, D., Feyen, J., 2004. Including prior information in the estimation of effective soil parameters in unsaturated zone modelling. *J. Hydrol.* 294 (4), 251–269.
- Merz, B., Plate, E.J., 1997. An analysis of the effects of spatial variability of soil and soil moisture on runoff. *Water Resour. Res.* 33 (12), 2909–2922.
- Mohamoud, Y.M., 1992. Evaluating Manning's roughness coefficients for tilled soils. *J. Hydrol.* 135 (1–4), 143–156.
- Morris, E.M., Woolhiser, D.A., 1980. Unsteady one-dimensional flow over a plane: partial equilibrium and recession hydrographs. *Water Resour. Res.* 16 (2), 355–360.
- Motha, J.A., Wigham, J.M., 1995. Modelling overland flow with seepage. *J. Hydrol.* 169 (1–4), 265–280.
- Nahar, N., Govindaraju, R.S., Corradini, C., Morbidelli, R., 2004. Role of run-on for describing field-scale infiltration and overland flow over spatially variable soils. *J. Hydrol.* 286 (1–4), 36–51.
- Panday, S., Huyakorn, P.S., 2004. A fully coupled physically-based spatially-distributed model for evaluating surface/subsurface flow. *Adv. Water Resour.* 27 (4), 361–382.
- Schwefel, H.P., 1993. Evolution and Optimum Seeking: The Sixth Generation. John Wiley & Sons, Inc., p. 456.
- Sepaskhah, A.R., Bondar, H., 2002. SW – soil and water: estimation of manning roughness coefficient for bare and vegetated furrow irrigation. *Biosyst. Eng.* 82 (3), 351–357.
- Šimunek, J., 2003. HYDRUS-2D Code Modification: Modeling Overland Flow. <<http://www.pc-progress.com/en/Default.aspx?h3d-overland>>.
- Šimunek, J., Sejna, M., van Genuchten, M.T., 1999. The HYDRUS-2D Software Package for Simulating Two-dimensional Movement of Water, Heat, and Multiple Solutes in Variably-saturated Media, Version 2.0. International Ground Water Modeling Center, Colorado School of Mines, Golden, Colorado.
- Šimunek, J., Jarvis, N.J., van Genuchten, M.T., Gärdenäs, A., 2003. Review and comparison of models for describing non-equilibrium and preferential flow and transport in the vadose zone. *J. Hydrol.* 272 (1–4), 14–35.
- Šimunek, J., van Genuchten, M.T., Sejna, M., 2008. Development and applications of the HYDRUS and STANMOD software packages and related codes. *Vadose Zone J.* 7 (2), 587–600.
- Singh, V., Bhallamudi, S.M., 1998. Conjoint surface–subsurface modeling of overland flow. *Adv. Water Resour.* 21 (7), 567–579.
- Singh, V.P., Jain, S.K., Sherif, M.M., 2005. Errors of kinematic wave and diffusion wave approximations for time-independent flows with infiltration and momentum exchange included. *Hydrol. Process.* 19 (9), 1771–1790.
- Tamari, S., Bruckler, L., Halbertsma, J., Chadoeuf, J., 1993. A simple method for determining soil hydraulic properties in the laboratory. *Soil Sci. Soc. Am. J.* 57 (3), 642–651.
- van Genuchten, M.T., 1980. A closed-form equation for predicting the hydraulic conductivity of unsaturated soils. *Soil Sci. Soc. Am. J.* 44 (5), 892–898.
- Vogel, H.J., Cousin, I., Ippisch, O., Bastian, P., 2005. The dominant role of structure for solute transport in soil: experimental evidence and modelling of structure and transport in a field experiment. *Hydrol. Earth Syst. Sci. Discuss.* 2 (5), 2153–2181.
- Vrugt, J.A., Robinson, B.A., 2007. Improved evolutionary optimization from genetically adaptive multimethod search. *Proc. Natl. Acad. Sci.* 104 (3), 708–711.
- Vrugt, J.A., Gupta, H.V., Bastidas, L.A., Bouten, W., Sorooshian, S., 2003. Effective and efficient algorithm for multiobjective optimization of hydrologic models. *Water Resour. Res.* 39 (8), 1214.
- Vrugt, J.A., Stauffer, P.H., Wöhling, T., Robinson, B.A., Vesselinov, V.V., 2008. Inverse modeling of subsurface flow and transport properties: a review with new developments. *Vadose Zone J.* 7 (2), 843–864.
- Wallach, R., Grigorin, G., Rivlin, J., 1997. The errors in surface runoff prediction by neglecting the relationship between infiltration rate and overland flow depth. *J. Hydrol.* 200 (1–4), 243–259.
- Wallach, R., Grigorin, G., Rivlin, J., 2001. A comprehensive mathematical model for transport of soil-dissolved chemicals by overland flow. *J. Hydrol.* 247 (1–2), 85–99.
- Wind, G.P., 1966. Capillary conductivity data estimated by a simple method. In: Rijtema, P.E., Wassink, H. (Eds.), *Water in the Unsaturated Zone*. IASH and UNESCO, Gentbrugge and Paris, pp. 181–191.

- Wöhling, T., Mailhol, J.C., 2007. Physically based coupled model for simulating 1D surface-2D subsurface flow and plant water uptake in irrigation furrows. II: model test and evaluation. *Journal of Irrigation and Drainage Engineering* 133 (6), 548–558.
- Wöhling, T., Schmitz, G.H., 2007. Physically based coupled model for simulating 1D surface-2D subsurface flow and plant water uptake in irrigation furrows. I: model development. *J. Irrigation Drainage Eng.* 133 (6), 538–547.
- Wöhling, T., Vrugt, J.A., 2008. Combining multiobjective optimization and Bayesian model averaging to calibrate forecast ensembles of soil hydraulic models. *Water Resour. Res.* 44 (12), W12432.
- Wöhling, T., Vrugt, J., in press. Multi-Response Multi-layer Vadose Zone Model Calibration using Markov Chain Monte Carlo Simulation and Field Water Retention Data. *Water Resources Research*, 47, WR009265.
- Wöhling, T., Vrugt, J.A., Barkle, G.F., 2008. Comparison of three multiobjective optimization algorithms for inverse modeling of vadose zone hydraulic properties. *Soil Sci. Soc. Am. J.* 72 (2), 305–319.
- Woolhiser, D.A., Smith, R.E., Goodrich, D.C., 1990. KINEROS, A Kinematic Runoff and Erosion Model: Documentation and User Manual.
- Zhang, Z.F., Ward, A.L., Gee, G.W., 2003. Estimating soil hydraulic parameters of a field drainage experiment using inverse techniques. *Vadose Zone J.* 2 (2), 201–211.